Hybrid quantum repeater for qudits

Marcel Bergmann and Peter van Loock
Institut für Physik, Johannes Gutenberg-Universität, Staudingerweg 7, 55128 Mainz, Germany

(Received 11 September 2017; published 29 March 2019)

We present a hybrid quantum repeater protocol for the long-distance distribution of atomic entangled states beyond qubits. In our scheme, imperfect noisy entangled pairs of two qudits, i.e., two discrete-variable d-level systems, each of, in principle, arbitrary dimension d, are initially shared between the intermediate stations of the channel. This is achieved via local, sufficiently strong light-matter interactions, involving optical coherent states and their transmission after these interactions, and optical measurements on the transmitted field modes, especially efficient continuous-variable homodyne detections ("hybrid" here refers to the simultaneous exploitation of discrete- and continuous-variable degrees of freedom for the local processing and storage of entangled states as well as their nonlocal distribution, respectively) and unambiguous state discrimination. For qutrits we quantify the light-matter entanglement that can be effectively shared through an elementary lossy channel, and for a repeater spacing of up to 10 km we show that the realistic (lossy) qutrit entanglement is even larger than any ideal (loss-free) qubit entanglement. After including qudit entanglement purification and swapping procedures, we calculate the long-distance entangled-pair distribution rates and the final entangled-state fidelities for total communication distances of up to 1280 km. For example, employing unambiguous state discrimination, with three rounds of purification, entangled qudit pairs of near-unit fidelity can be distributed over 1280 km at an ideal maximal rate (assuming perfect gate operations) on the order of 100 Hz.

DOI: 10.1103/PhysRevA.99.032349

I. INTRODUCTION

Long-distance quantum communication is one of the most challenging tasks in practical quantum information. For future quantum networks, the distribution of entanglement between widely separated parties is necessary to make teleportation and secure communication over long distances possible. In practice, however, the direct transmission of quantum information or entangled states is typically performed by sending light through a lossy quantum channel (an optical fiber), which leads to an exponential decay of the success rate or the fidelity. To overcome this problem, quantum repeaters were proposed [1–3].

From the perspective of the most recent quantum repeater research, a quantum repeater protocol can be classified into three distinct categories, referred to as quantum repeater generations [4,5]. Though much slower compared to second- and third-generation quantum repeaters based on quantum error correction of, respectively, local (operation and memory) or transmission errors, first-generation quantum repeaters are attractive due to their immediate experimental feasibility (however, for a potentially practical approach to a third-generation quantum repeater based on static linear optics and certain multi-photon entangled states, see [6,7]). In first-generation quantum repeaters, by means of entanglement swapping [8], the distribution of long-distance entanglement is achieved via initial short-distance entanglement distributions. Hence, for the realization of first-generation quantum repeater schemes, the heralded generation of short-distance entanglement and the availability of quantum memories are essential prerequisites.

A prominent instance of a first-generation quantum repeater scheme is the well-known Duan-Lukin-Cirac-Zoller (DLCZ) protocol [9], which employs atomic ensembles as quantum memories and single photons with linear optics for entanglement distribution and swapping. A remarkable feature of the DLCZ scheme is that the so-called purification of entanglement, turning imperfect mixed entangled states into purer (in principle, perfect) versions of entangled states, is built into the process of entanglement distribution and swapping (purifying the entangled atomic ensembles from the effects of transmission and memory losses, respectively). Otherwise, in a standard first-generation quantum repeater [1,2], quantum error detection must be included via additional rounds of entanglement purification acting on two or more copies of entangled states and employing local quantum logic (together with two-way classical communication). Second-generation schemes use quantum error correction against memory errors, while in third-generation quantum repeaters memories are no longer necessary [10] since, for example, suitably encoded quantum information is directly sent through the channel [4–7]. A conceptually distinct version of such a loss-error-correction-based repeater is the all-optical scheme of Azuma *et al.* [11] based on the distribution of entangled cluster states. This scheme also relies on sufficiently fast feedforward operations (as opposed to the all-optical scheme of [6,7]).

All experimental demonstrations to date are for elements of a first-generation repeater, although light-matter interfaces and/or memories are still too inefficient to exceed the bounds [12–14] of repeaterless quantum communication (or to even scale up a repeater to really large distances). In fact, many quantum memories that have been demonstrated so far perform worse compared to a simple optical fiber loop [15].

A first-generation so-called hybrid quantum repeater (HQR) protocol for the distribution of atomic qubit-qubit

entanglement was given in [16–18]. Similar to other hybrid quantum information processing schemes [19], this protocol combines the advantages of discrete- and continuous-variable quantum states. Atomic two-level systems with long coherence time serve as quantum memories, while optical coherent states are used to generate the initial entanglement between the atoms using dispersive light-matter interactions and, in particular, highly efficient homodyne measurements. Employing such Gaussian measurements and Gaussian states as the initial resources appears very attractive from a practical point of view compared to repeater schemes based on the generation and detection of single photons. A particular experimental approach to this scheme, based on ions, was considered in [20]. Another, similar HQR protocol can be found in [21] and a recent hybrid approach to entanglement swapping using coherent states and linear optics is presented in [22].

On the fundamental level, higher-dimensional quantum systems of dimension d, so-called qudits, do not only play an important role in closing of the detection loophole in Bell test experiments [23,24]. In addition, it has been shown in [25] that qudits lead to an increase in data transfer and especially to a higher security in quantum key distribution (QKD) [26] compared to schemes involving only qubits [27]. One possibility to realize such improved schemes is the initial distribution of high-dimensional entanglement using correspondingly high-dimensional quantum repeaters, which is the topic of this paper.[1] Despite the many existing works on qubit quantum repeaters, rather little attention has been paid to qudit quantum repeaters aiming at the long-distance distribution of qudit entanglement and information.

In this paper we generalize the HQR protocol for the distribution of qubit-qubit entanglement [16,17] to the case of qudit-qudit entanglement, i.e., bipartite states of multilevel systems. The structure of the paper is as follows. In Sec. II we review the HQR protocol for the qubit case and adapt it to our later generalization for qudits. In Sec. III we generalize this scheme to the case of three-level systems (qutrits). After proposing a generalized dispersive qutrit-light interaction, we discuss the process of entanglement generation in elementary links using this interaction. We consider both homodyne detection and unambiguous state discrimination for the measurement on the light mode. Including entanglement purification for the initial qutrit-qutrit entangled states, we calculate the final rates and fidelities for our generalized entanglement distribution scheme in various scenarios. Based on these results, in Sec. IV we discuss a further generalization to arbitrarily (finite) dimensional quantum systems before we conclude in Sec. V.

[1]Note that inferring from the results of Refs. [12–14], e.g., the effective secret bit rate in a long-distance QKD scheme based on direct state transmissions cannot be improved beyond that of, for instance, a qubit-based BB84 scheme. Thus, on a fundamental level, beyond-qubit-type encodings do not seem to be particularly useful for direct long-distance QKD applications. Nonetheless, when employing quantum repeaters, switching to qudits may indeed be useful.

II. HYBRID QUANTUM REPEATER FOR QUBITS

The physical setup for a qubit HQR is as follows. The qubit is represented by the two spin states $|0\rangle$ and $|1\rangle$ of an atomic electron. The atom is placed into a cavity and the electronic spin interacts with a bright coherent-state light pulse. The situation at hand is theoretically described by the Jaynes-Cummings model in the limit of large detuning [28], i.e., the probe pulse and the cavity are in resonance, but both are detuned from the resonance frequency of the electronic transition.

The interaction Hamiltonian in this model reads $H_{\text{int}}^{(2)} = \hbar g \sigma_z a^\dagger a$, where $\sigma_z = -\frac{1}{2}|0\rangle\langle 0| + \frac{1}{2}|1\rangle\langle 1|$ corresponds to a Pauli operator on the spin state and $a^\dagger a$ is the photon-number operator of the light mode. Furthermore, the parameter g describes the strength of the spin-light coupling.

Based on this interaction Hamiltonian, the corresponding unitary transformation is given by $U_2(\theta) = \exp(i\theta\sigma_z a^\dagger a)$ (with an effective interaction time $\theta = gt$) and, up to an unconditional phase shift of the mode by $e^{i\theta/2}$, acts on the spin-light system effectively as a controlled phase rotation, i.e.,

$$U_2(\theta)[(|0\rangle + |1\rangle) \otimes |\alpha\rangle] = |0\rangle|\alpha\rangle + |1\rangle|\alpha e^{i\theta}\rangle. \quad (1)$$

In the literature, this interaction is also known as dispersive interaction [29]. For the generalization that we are aiming at, we consider the case $\theta = \pi$, corresponding to a strong interaction resulting in coherent states $|\pm\alpha\rangle$ on the light mode.

The repeater protocol now works as follows. The matter system is prepared in the state $|0\rangle + |1\rangle$ and interacts dispersively with a single-mode coherent state $|\alpha\rangle$ (referred to as a qubus) as described by Eq. (1). Note that this leads to a pure (effectively qubit-qubit) entangled state between the light mode and the matter system.

The light mode is then sent through an optical channel where it inevitably suffers from photon loss. The photon loss can be modeled by mixing the light mode with a vacuum state at a beam splitter with transmittance γ, where $1-\gamma$ is related to the loss probability of a single photon. It is also related to the optical propagation distance L, i.e., $\gamma = \exp(-\frac{L}{L_{\text{att}}})$ with the attenuation length $L_{\text{att}} \approx 22$ km for photons at telecom wavelength.

After applying the beam splitter, the total pure state of the matter system, the qubus light mode, and the loss mode read

$$\frac{1}{\sqrt{2}}(|0\rangle|\sqrt{\gamma}\alpha\rangle|\sqrt{1-\gamma}\alpha\rangle + |1\rangle|-\sqrt{\gamma}\alpha\rangle|-\sqrt{1-\gamma}\alpha\rangle). \quad (2)$$

The relevant joint state of the matter system and the light mode is obtained by tracing out the loss mode. Since the coherent states $|\alpha\rangle$ and $|-\alpha\rangle$ are not orthogonal, it is useful to transform these into an orthogonal basis. A suitable orthogonal basis in this case is the basis of even and odd Schrödinger cat states (throughout we assume $\alpha \in \mathbb{R}$),

$$|u\rangle = \frac{1}{\sqrt{N_u(\alpha)}}(|\alpha\rangle + |-\alpha\rangle), \quad (3)$$

$$|v\rangle = \frac{1}{\sqrt{N_v(\alpha)}}(|\alpha\rangle - |-\alpha\rangle), \quad (4)$$

with normalization constants $N_u(\alpha) = 2(1 + e^{-2\alpha^2})$ and $N_v(\alpha) = 2(1 - e^{-2\alpha^2})$. Expressed in this basis, one has

$$|\alpha\rangle = \tfrac{1}{2}(\sqrt{N_u(\alpha)}|u\rangle + \sqrt{N_v(\alpha)}|v\rangle), \tag{5}$$

$$|-\alpha\rangle = \tfrac{1}{2}(\sqrt{N_u(\alpha)}|u\rangle - \sqrt{N_v(\alpha)}|v\rangle). \tag{6}$$

After tracing out the loss mode in this basis, the resulting state of the matter system and the qubus light mode becomes

$$\begin{aligned}\rho_{\text{out}} = {} & \frac{N_u(\sqrt{1-\gamma}\alpha)}{4}\left[\frac{1}{\sqrt{2}}(|0\rangle|\sqrt{\gamma}\alpha\rangle + |1\rangle|-\sqrt{\gamma}\alpha\rangle)\right] \times \text{H.c.} \\ & + \frac{N_v(\sqrt{1-\gamma}\alpha)}{4} \\ & \times \left[\frac{1}{\sqrt{2}}(|0\rangle|\sqrt{\gamma}\alpha\rangle - |1\rangle|-\sqrt{\gamma}\alpha\rangle)\right] \times \text{H.c.}\end{aligned} \tag{7}$$

This is a mixed entangled state between the matter system (the atomic qubit) and the qubus. To study the entanglement of such a state and also for later purposes, it is most convenient to use directly the $|\tilde{u}\rangle$, $|\tilde{v}\rangle$ basis on the light mode, where the tilde refers to the basis vectors in Eqs. (3) and (4) with damped amplitudes $\sqrt{\gamma}\alpha$.

In addition, a basis change on the matter-qubit system into the conjugate (Pauli) X basis, $|\tilde{0}\rangle = \frac{1}{\sqrt{2}}(|0\rangle + |1\rangle)$ and $|\tilde{1}\rangle = \frac{1}{\sqrt{2}}(|0\rangle - |1\rangle)$, gives the expression

$$\begin{aligned}\rho_{\text{out}} = {} & \frac{N_u(\sqrt{1-\gamma}\alpha)}{4}\left[\frac{1}{2}\left(\sqrt{N_u(\sqrt{\gamma}\alpha)}|\tilde{0}\rangle|\tilde{u}\rangle\right.\right. \\ & \left.\left. + \sqrt{N_v(\sqrt{\gamma}\alpha)}|\tilde{1}\rangle|\tilde{v}\rangle\right)\right] \times \text{H.c.} \\ & + \frac{N_v(\sqrt{1-\gamma}\alpha)}{4}\left[\frac{1}{2}\left(\sqrt{N_u(\sqrt{\gamma}\alpha)}|\tilde{1}\rangle|\tilde{u}\rangle\right.\right. \\ & \left.\left. + \sqrt{N_v(\sqrt{\gamma}\alpha)}|\tilde{0}\rangle|\tilde{v}\rangle\right)\right] \times \text{H.c.},\end{aligned} \tag{8}$$

which now represents the state in Eq. (7) in suitable binary orthogonal bases for both the matter system and the qubus. Note that this does not change the entanglement properties of the state since any entanglement measure is invariant under local basis changes [30–32]. Also note that this matter-light qubit-qubus entangled state effectively remains an entangled qubit-qubit state, since the two initial coherent states of the qubus span a two-dimensional qubit space and because individual coherent states remain pure after a loss channel.

After traveling through an optical fiber over the distance L_0, the light mode interacts dispersively with a second matter-qubit system, also prepared in the state $|0\rangle + |1\rangle$, but this time with the inverse angle $\theta = -\pi$. The joint tripartite state, written in the same bases as in Eq. (7), then becomes

$$\rho'_{\text{out}} = \frac{N_u(\sqrt{1-\gamma}\alpha)}{4}|C_0\rangle\langle C_0| + \frac{N_v(\sqrt{1-\gamma}\alpha)}{4}|C_1\rangle\langle C_1|, \tag{9}$$

where

$$|C_0\rangle = \frac{1}{\sqrt{2}}(|\phi^+\rangle|\sqrt{\gamma}\alpha\rangle + |\psi^+\rangle|-\sqrt{\gamma}\alpha\rangle) \tag{10}$$

and

$$|C_1\rangle = \frac{1}{\sqrt{2}}(|\phi^-\rangle|\sqrt{\gamma}\alpha\rangle + |\psi^-\rangle|-\sqrt{\gamma}\alpha\rangle). \tag{11}$$

Here we introduced the qubit Bell states

$$|\phi^\pm\rangle = \frac{1}{\sqrt{2}}(|00\rangle \pm |11\rangle), \quad |\psi^\pm\rangle = \frac{1}{\sqrt{2}}(|10\rangle \pm |01\rangle). \tag{12}$$

The component $|C_0\rangle$ in Eq. (9) is the desired target component, whereas $|C_1\rangle$ is the loss component that vanishes in the loss-free case. Indeed, for $\gamma \to 1$, one observes $N_u(0) = 4$ and $N_v(0) = 0$ such that in this case the corresponding output density operator $\rho'_{\text{out}} = |C_0\rangle\langle C_0|$ represents a pure state. Opposed to the original HQR for qubits [17], here every term in $|C_0\rangle$ contains matter two-qubit entanglement because of our choice $\theta = \pm\pi$. This choice will enable us later to obtain a natural generalization to qudits. To achieve the goal of distributing entanglement between the two separated matter systems over the distance L_0, the final step is a measurement on the light mode, for instance, by homodyne detection. Unlike in the original HQR protocol [17], where the dispersive interaction is assumed to be weak (and hence a p-homodyne detection is ultimately preferred over an x-homodyne detection with, respectively, state distinguishabilities $\sim\alpha\theta$ versus $\alpha\theta^2$ for small but otherwise unfixed θ), a suitable detection scheme in our case for strong and fixed $\theta = \pm\pi$ is a measurement of the quadrature $\hat{x} = \frac{1}{2}(a + a^\dagger)$ instead of $\hat{p} = \frac{1}{2i}(a - a^\dagger)$.

The position distribution of coherent states with complex amplitude β can be obtained by the square of their position wave functions

$$|\psi_\beta(x)|^2 = \sqrt{\frac{2}{\pi}}\exp\{-2[x - \text{Re}(\beta)]^2\}. \tag{13}$$

Because of the finite overlap of the coherent states $|\sqrt{\gamma}\alpha\rangle$ and $|-\sqrt{\gamma}\alpha\rangle$, it is impossible to perfectly distinguish these states and an error due to this nonorthogonality has to be taken into account. Based on Eq. (13), it is obvious that $|\sqrt{\gamma}\alpha\rangle$ and $|-\sqrt{\gamma}\alpha\rangle$ have Gaussian position distributions around $\sqrt{\gamma}\alpha$ and $-\sqrt{\gamma}\alpha$, respectively. It is therefore useful to assign the result of the x measurement to one of three possible windows.

The first window is $w_0 = [\sqrt{\gamma}\alpha - \Delta, \infty]$ with $\sqrt{\gamma}\alpha > \Delta > 0$. If the measurement result falls in this range, then the light mode is effectively projected onto $|\sqrt{\gamma}\alpha\rangle$. Note that this is an approximate projection due to the nonorthogonality, i.e., the resulting reduced state for the two matter qubits is still a superposition of $|\phi^+\rangle$ and $|\psi^+\rangle$ in the first (target) component, while the weight of $|\psi_+\rangle$ can be reduced by increasing the value of $\sqrt{\gamma}\alpha$. The same is true in the second component for $|\phi^-\rangle$ and $|\psi^-\rangle$.

As for the second window, we define $w_1 = [-\infty, -\sqrt{\gamma}\alpha + \Delta]$, which is symmetric to w_0 and therefore represents the approximate projection on $|-\sqrt{\gamma}\alpha\rangle$. Unlike w_0, one has now $|\psi^\pm\rangle$ as the dominant terms in the superpositions in the two components. It is again true that the nondominant term in the superposition can be made arbitrarily small by increasing $\sqrt{\gamma}\alpha$. A third window w_2 can be defined in between w_0 and w_1, and a measurement result in this range will be considered as a failure event to be discarded (see Fig. 1). Useful figures of merit for the performance

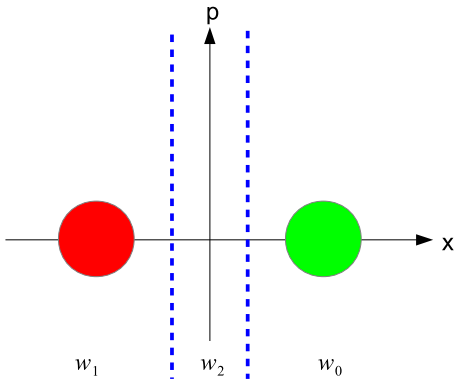

FIG. 1. Phase-space representation of two coherent states $|\sqrt{\gamma}\alpha\rangle$ and $|-\sqrt{\gamma}\alpha\rangle$ to be distinguished by homodyne detection. The measurement window w_2 includes all failure events that are discarded.

of this entanglement distribution scheme are the success probabilities for the two nonfailure windows w_0 and w_1 as well as the fidelity of the corresponding target state in the first component. As the fidelity, we define the overlap of the maximally entangled Bell states $|\phi^+\rangle$ (w_0) or $|\psi^+\rangle$ (w_1) with the (reduced) mixed state in Eq. (9) after the corresponding homodyne measurement outcome for the light mode.

The success probability for a measurement result to fall in the first window reads

$$p_{w_0} = \frac{1}{2}\int_{\sqrt{\gamma}\alpha-\Delta}^{\infty} dx[|\psi_{\sqrt{\gamma}\alpha}(x)|^2 + |\psi_{-\sqrt{\gamma}\alpha}(x)|^2]. \quad (14)$$

For the second window we have

$$p_{w_1} = \frac{1}{2}\int_{-\infty}^{-\sqrt{\gamma}\alpha+\Delta} dx[|\psi_{\sqrt{\gamma}\alpha}(x)|^2 + |\psi_{-\sqrt{\gamma}\alpha}(x)|^2], \quad (15)$$

which equals p_{w_0} for symmetry reasons. The same holds true for the two fidelities

$$\begin{aligned} F_{w_0} &= F_{w_1} \\ &= \frac{N_u(\sqrt{1-\gamma}\alpha)}{4} \\ &\quad \times \frac{\int_{-\infty}^{-\sqrt{\gamma}\alpha+\Delta} dx|\psi_{-\sqrt{\gamma}\alpha}(x)|^2}{\int_{-\infty}^{-\sqrt{\gamma}\alpha+\Delta} dx[|\psi_{\sqrt{\gamma}\alpha}(x)|^2 + |\psi_{-\sqrt{\gamma}\alpha}(x)|^2]}. \end{aligned} \quad (16)$$

The formulas for the fidelities and the success probabilities imply the crucial dependence of the performance on the choice of Δ and $\sqrt{\gamma}\alpha$: If we choose $\Delta = \Delta_0 := \sqrt{\gamma}\alpha$, then we have no failure window and every measurement result is assigned to one of the two coherent states $|\pm\sqrt{\gamma}\alpha\rangle$. The corresponding success probability equals unity at the expense of a rather low fidelity. With $\Delta < \Delta_0$, the success probability is clearly less than unity and the fidelity increases correspondingly.

In general, the fidelity drops for too small $\sqrt{\gamma}\alpha$ due to the nonorthogonality and thus indistinguishability of the coherent states $|\pm\sqrt{\gamma}\alpha\rangle$. The overall effect becomes manifest in bit-flip errors in the target Bell states. Though leading to near orthogonality, large amplitudes $\sqrt{\gamma}\alpha$ result in a near-equal mixture of the state in Eq. (9) which then, after a near-deterministic discrimination, consists of one of the two possible Bell states in the first component and its phase-flipped version in the second component. This state therefore has very low entanglement and hence is of limited practical interest. So the task is to find a regime of α and distances L_0 such that both reasonable fidelities and success probabilities can be obtained.

Besides homodyne detection, unambiguous state discrimination (USD) has been considered for hybrid quantum repeaters in the literature [16]. The advantage here is that the effects originating from the finite overlaps of the coherent states no longer appear in the fidelity due to an error-free state discrimination. The corresponding effects solely influence the success probabilities depending on the weights of the inconclusive discrimination results. Two-state USD for coherent states $|\pm\sqrt{\gamma}\alpha\rangle$ is well known and can be optimally performed via a single beam splitter and on-off detections [33].

Further steps in the original repeater protocol address the purification of the mixed state in Eq. (9) after homodyne detection and entanglement swapping on the matter system or via the qubus to distribute the generated entanglement over longer distances. For more details, see, e.g., [16].

III. HYBRID QUANTUM REPEATER FOR QUTRITS

A. Dispersive light-matter interaction

The dispersive interaction [see Eq. (1)] lies at the heart of the HQR for qubits and therefore, as a first step to extend this repeater scheme to qutrits, a generalization of the dispersive interaction to the qutrit case is necessary. In analogy to the dispersive interaction for qubits, we define the qutrit-qubus interaction Hamiltonian as

$$H_{\text{int}}^{(3)} = \hbar g S_z^{(3)} a^\dagger a, \quad (17)$$

where the operator $S_z^{(3)}$ acts on the qutrit basis states $|0\rangle$, $|1\rangle$, and $|2\rangle$ as

$$S_z^{(3)}|0\rangle = -1|0\rangle, \quad S_z^{(3)}|1\rangle = 0|1\rangle, \quad S_z^{(3)}|2\rangle = 1|2\rangle. \quad (18)$$

The matter system could be realized, for example, by a spin-1 particle where the basis states are the eigenstates with the corresponding magnetic quantum numbers $m_z = -1, 0, 1$. Such a spin realization of a qutrit has been demonstrated in the framework of nuclear magnetic resonance for various applications [34,35].

Similar to the qubit case, the corresponding unitary transformation is $U_3(\theta) = \exp(i\theta S_z^{(3)} a^\dagger a)$, which again corresponds to a conditional phase rotation on the light-matter system (up to an unconditional phase shift of the qubus mode by $e^{i\theta}$), i.e.,

$$\begin{aligned} &U_3(\theta)[(|0\rangle + |1\rangle + |2\rangle) \otimes |\alpha\rangle] \\ &\quad = |0\rangle|\alpha\rangle + |1\rangle|\alpha e^{i\theta}\rangle + |2\rangle|\alpha e^{2i\theta}\rangle. \end{aligned} \quad (19)$$

For our purposes, we will choose $\theta = \frac{2\pi}{3}$ to obtain a rather strong dispersive interaction.

B. Loss-free case

The qutrit hybrid repeater protocol works in complete analogy to the qubit case. To illustrate the concept, we first omit photon losses in the optical fiber and assume a noiseless quantum channel.

The repeater protocol works as follows. First, the matter system is initiated in the state $\frac{1}{\sqrt{3}}(|0\rangle + |1\rangle + |2\rangle)$ and interacts with a light mode in a coherent state $|\alpha\rangle$ via the qutrit dispersive interaction with $\theta = \frac{2\pi}{3}$. This results in the entangled matter-qubus state

$$\frac{1}{\sqrt{3}}(|0\rangle|\alpha\rangle + |1\rangle|\alpha e^{2\pi i/3}\rangle + |2\rangle|\alpha e^{-2\pi i/3}\rangle). \tag{20}$$

The light mode is then sent to a second matter system, separated from the first one by a distance L_0 and also prepared in the state $\frac{1}{\sqrt{3}}(|0\rangle + |1\rangle + |2\rangle)$. The incoming light mode interacts dispersively with the second matter system, but this time with the reverse angle $\theta = -\frac{2\pi}{3}$. The resulting pure state is

$$\begin{aligned}\frac{1}{\sqrt{3}}\Bigg(&\frac{1}{\sqrt{3}}(|00\rangle + |11\rangle + |22\rangle)|\alpha\rangle \\ &+ \frac{1}{\sqrt{3}}(|02\rangle + |10\rangle + |21\rangle)|\alpha e^{2\pi i/3}\rangle \\ &+ \frac{1}{\sqrt{3}}(|01\rangle + |12\rangle + |20\rangle)|\alpha e^{-2\pi i/3}\rangle\Bigg).\end{aligned} \tag{21}$$

To keep the notation short and also for later purposes, it it useful to define the set of maximally entangled qutrit Bell states

$$|\phi_{kj}\rangle = \frac{1}{\sqrt{3}}\sum_{m=0}^{2}\exp\left(\frac{2\pi i k m}{3}\right)|m, m \ominus j\rangle, \tag{22}$$

where $\ominus$ denotes subtraction modulo 3 and $k, j = 0, 1, 2$. Equation (21) can therefore be rewritten as

$$\frac{1}{\sqrt{3}}(|\phi_{00}\rangle|\alpha\rangle + |\phi_{01}\rangle|\alpha e^{2\pi i/3}\rangle + |\phi_{02}\rangle|\alpha e^{-2\pi i/3}\rangle). \tag{23}$$

To generate a maximally entangled state between the matter systems, a homodyne measurement is performed on the light mode to distinguish the three coherent states of the mode (see Fig. 2). Unlike the qubit case, here a measurement of $\hat{p}$ is useful, because it allows one to (almost) discriminate all three coherent states (as opposed to the case of an $\hat{x}$ measurement). Moreover, for an ideal loss-free channel, increasing the amplitude α leads to near orthogonality of the coherent states such that a perfect, near maximally entangled qutrit-qutrit state can be deterministically distributed over the distance L_0. To further extend the entanglement, two such elementary pairs next to each other are connected by entanglement swapping, via a Bell measurement on adjacent repeater nodes. By one successful entanglement swapping step, qutrit-qutrit entanglement can thus be shared over the distance $2L_0$, and so forth.

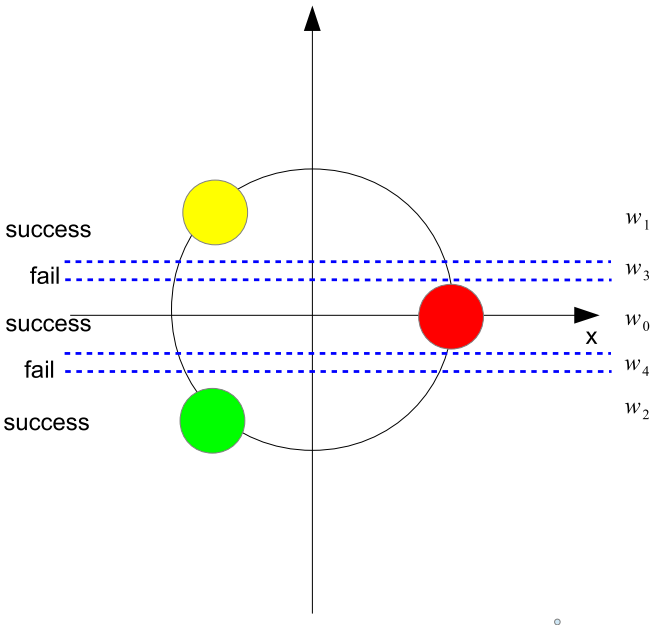

FIG. 2. Phase-space representation of the three coherent states $|\alpha\rangle$ and $|\alpha e^{\pm 2\pi i/3}\rangle$ to be distinguished by homodyne detection.

We will address all the steps of the qutrit repeater protocol in detail in the following sections and also explain which subtleties and necessary generalizations occur in practice compared to the idealized loss-free case discussed here.

C. Matter-light qutrit-qubus hybrid entanglement

At the beginning of the qutrit HQR protocol, the matter system is prepared in the state $\frac{1}{\sqrt{3}}(|0\rangle + |1\rangle + |2\rangle)$. The dispersive interaction with a coherent state leads to the state in Eq. (20). In the realistic case, the light mode is sent through an optical loss channel (e.g., an optical fiber), which is again simulated by a coupling of the mode with an ancilla vacuum state. This time, the application of the beam splitter leads to

$$\frac{1}{\sqrt{3}}(|0\rangle|\sqrt{\gamma}\alpha\rangle|\sqrt{1-\gamma}\alpha\rangle + |1\rangle|\sqrt{\gamma}\alpha e^{2\pi i/3}\rangle|\sqrt{1-\gamma}\alpha e^{2\pi i/3}\rangle + |2\rangle|\sqrt{\gamma}\alpha e^{-2\pi i/3}\rangle|\sqrt{1-\gamma}\alpha e^{-2\pi i/3}\rangle). \tag{24}$$

To trace out the loss mode, it is again useful to switch to an orthogonal basis. While in the qubit case that basis is given by a kind of coherent-state qubit Hadamard transform, the qutrit basis is given by a kind of coherent-state qutrit Hadamard gate to yield

$$\begin{aligned}|u\rangle &= \frac{1}{\sqrt{N_u(\alpha)}}(|\alpha\rangle + |\alpha e^{2\pi i/3}\rangle + |\alpha e^{-2\pi i/3}\rangle), \\ |v\rangle &= \frac{1}{\sqrt{N_v(\alpha)}}(|\alpha\rangle + e^{2\pi i/3}|\alpha e^{2\pi i/3}\rangle + e^{-2\pi i/3}|\alpha e^{-2\pi i/3}\rangle), \\ |w\rangle &= \frac{1}{\sqrt{N_w(\alpha)}}(|\alpha\rangle + e^{-2\pi i/3}|\alpha e^{2\pi i/3}\rangle + e^{2\pi i/3}|\alpha e^{-2\pi i/3}\rangle),\end{aligned} \tag{25}$$

with normalization constants

$$\begin{aligned} N_u(\alpha) &= 3 + 6e^{-(3/2)\alpha^2}\cos\left(\sqrt{\tfrac{3}{4}}\alpha^2\right), \\ N_v(\alpha) &= 3 - e^{-(3/2)\alpha^2}\left[3\cos\left(\sqrt{\tfrac{3}{4}}\alpha^2\right) + \sqrt{3}\sin\left(\sqrt{\tfrac{3}{4}}\alpha^2\right)\right], \\ N_w(\alpha) &= 3 - e^{-(3/2)\alpha^2}\left[3\cos\left(\sqrt{\tfrac{3}{4}}\alpha^2\right) - \sqrt{3}\sin\left(\sqrt{\tfrac{3}{4}}\alpha^2\right)\right]. \end{aligned} \tag{26}$$

The coherent states above can thus be written as

$$\begin{aligned} |\alpha\rangle &= \tfrac{1}{3}[\sqrt{N_u(\alpha)}|u\rangle + \sqrt{N_v(\alpha)}|v\rangle + \sqrt{N_w(\alpha)}|w\rangle], \\ |\alpha e^{2\pi i/3}\rangle &= \tfrac{1}{3}[\sqrt{N_u(\alpha)}|u\rangle + e^{-2\pi i/3}\sqrt{N_v(\alpha)}|v\rangle + e^{2\pi i/3}\sqrt{N_w(\alpha)}|w\rangle], \\ |\alpha e^{-2\pi i/3}\rangle &= \tfrac{1}{3}[\sqrt{N_u(\alpha)}|u\rangle + e^{2\pi i/3}\sqrt{N_v(\alpha)}|v\rangle + e^{-2\pi i/3}\sqrt{N_w(\alpha)}|w\rangle]. \end{aligned} \tag{27}$$

Substituting this into Eq. (24) for the loss mode and tracing out the loss mode gives the three-component mixed state

$$\begin{aligned} \rho_{\text{out}} = {} & \frac{N_u(\sqrt{1-\gamma}\alpha)}{9}\left[\frac{1}{\sqrt{3}}(|0\rangle|\sqrt{\gamma}\alpha\rangle + |1\rangle|\sqrt{\gamma}\alpha e^{2\pi i/3}\rangle + |2\rangle|\sqrt{\gamma}\alpha e^{-2\pi i/3}\rangle)\right] \times \text{H.c.} \\ & + \frac{N_v(\sqrt{1-\gamma}\alpha)}{9}\left[\frac{1}{\sqrt{3}}(|0\rangle|\sqrt{\gamma}\alpha\rangle + e^{-2\pi i/3}|1\rangle|\sqrt{\gamma}\alpha e^{2\pi i/3}\rangle + e^{2\pi i/3}|2\rangle|\sqrt{\gamma}\alpha e^{-2\pi i/3}\rangle)\right] \times \text{H.c.} \\ & + \frac{N_w(\sqrt{1-\gamma}\alpha)}{9}\left[\frac{1}{\sqrt{3}}(|0\rangle|\sqrt{\gamma}\alpha\rangle + e^{2\pi i/3}|1\rangle|\sqrt{\gamma}\alpha e^{2\pi i/3}\rangle + e^{-2\pi i/3}|2\rangle|\sqrt{\gamma}\alpha e^{-2\pi i/3}\rangle)\right] \times \text{H.c.} \end{aligned} \tag{28}$$

This represents an entangled state between the qutrit matter system and the qubus. Similar to the qubit case, the resulting density matrix still effectively represents a state of two qutrits (one optical and one material), since the three coherent states $\{|\sqrt{\gamma}\alpha\rangle, |\sqrt{\gamma}\alpha e^{\pm 2\pi i/3}\rangle\}$ effectively span a three-dimensional Hilbert space.

For studying the entanglement properties of ρ_{out}, it is helpful to express the light mode in the $\{|u\rangle, |v\rangle, |w\rangle\}$ basis and the matter system in the qutrit (generalized Pauli) X basis,

$$|\tilde{0}\rangle = \frac{1}{\sqrt{3}}(|0\rangle + |1\rangle + |2\rangle), \quad |\tilde{1}\rangle = \frac{1}{\sqrt{3}}(|0\rangle + e^{2\pi i/3}|1\rangle + e^{-2\pi i/3}|2\rangle), \quad |\tilde{2}\rangle = \frac{1}{\sqrt{3}}(|0\rangle + e^{-2\pi i/3}|1\rangle + e^{2\pi i/3}|2\rangle). \tag{29}$$

Equation (28) can thus be rewritten as

$$\begin{aligned} \rho_{\text{out}} = {} & \frac{N_u(\sqrt{1-\gamma}\alpha)}{9}\left[\frac{1}{3}(\sqrt{N_u(\sqrt{\gamma}\alpha)}|\tilde{0}\rangle|\tilde{u}\rangle + \sqrt{N_v(\sqrt{\gamma}\alpha)}|\tilde{1}\rangle|\tilde{v}\rangle + \sqrt{N_w(\sqrt{\gamma}\alpha)}|\tilde{2}\rangle|\tilde{w}\rangle)\right] \times \text{H.c.} \\ & + \frac{N_v(\sqrt{1-\gamma}\alpha)}{9}\left[\frac{1}{3}(\sqrt{N_u(\sqrt{\gamma}\alpha)}|\tilde{2}\rangle|\tilde{u}\rangle + \sqrt{N_v(\sqrt{\gamma}\alpha)}|\tilde{1}\rangle|\tilde{v}\rangle + \sqrt{N_w(\sqrt{\gamma}\alpha)}|\tilde{0}\rangle|\tilde{w}\rangle)\right] \times \text{H.c.} \\ & + \frac{N_w(\sqrt{1-\gamma}\alpha)}{9}\left[\frac{1}{3}(\sqrt{N_u(\sqrt{\gamma}\alpha)}|\tilde{1}\rangle|\tilde{u}\rangle + \sqrt{N_v(\sqrt{\gamma}\alpha)}|\tilde{0}\rangle|\tilde{v}\rangle + \sqrt{N_w(\sqrt{\gamma}\alpha)}|\tilde{2}\rangle|\tilde{w}\rangle)\right] \times \text{H.c.}, \end{aligned} \tag{30}$$

where $|\tilde{u}\rangle$, $|\tilde{v}\rangle$, and $|\tilde{w}\rangle$ denote the basis vectors in Eq. (25) with amplitudes $\sqrt{\gamma}\alpha$.

To quantify the qutrit-qutrit entanglement of this state, we choose the so-called entanglement negativity [36,37] as our figure of merit. The negativity $\mathcal{N}$ of a bipartite quantum state of a system AB is defined as

$$\mathcal{N}(\rho) = \frac{\|\rho^{T_A}\| - 1}{2}, \tag{31}$$

where ρ^{T_A} is the partial transposition of the bipartite state with respect to system A and $\|\cdot\|$ denotes the trace norm.

A plot of the negativities for different initial amplitudes α and various elementary distances L_0 with $\gamma = \exp(-\frac{L_0}{L_{\text{att}}})$ is shown in Fig. 3. The dashed orange line indicates the entanglement negativity of a pure maximally entangled qubit Bell state. Up to a distance of approximately $L_0 = 10$ km, it is possible to generate matter-qubus entanglement stronger than any, even ideal qubit-qubit entanglement. Taking into account that the realistic distribution of qubit-qubit entanglement is also subject to loss, the difference in entanglement negativity will be even more significant. However, a crucial step still is to transfer this entanglement to a sufficient extent from the matter-light system to a matter-matter system for storage.

D. Matter-matter qutrit-qutrit entanglement

To distribute entanglement between two matter qutrits, the light mode of the state in Eq. (28) interacts with a second matter system, initialized in the state $\frac{1}{\sqrt{3}}(|0\rangle + |1\rangle + |2\rangle)$. This time, similar to the qubit case, the controlled phase

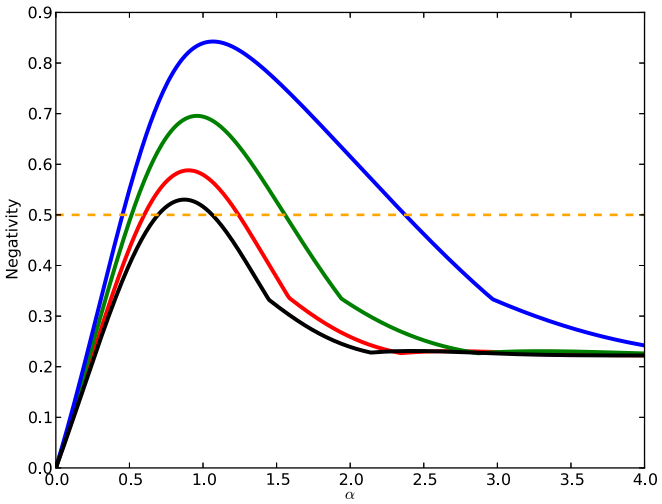

FIG. 3. Negativity of the effective qutrit-qutrit state dependent on α for various distances: 10 km (black line), 8 km (red line), 5 km (green line), and 2 km (blue line) (from bottom to top). The orange dashed line indicates the negativity of a maximally entangled pure two-qubit Bell state.

rotation takes place with the opposite angle $\theta = -\frac{2\pi}{3}$. One obtains

$$\rho'_{\text{out}} = \frac{N_u(\sqrt{1-\gamma}\alpha)}{9}|C_0\rangle\langle C_0| + \frac{N_v(\sqrt{1-\gamma}\alpha)}{9}|C_1\rangle\langle C_1| + \frac{N_w(\sqrt{1-\gamma}\alpha)}{9}|C_2\rangle\langle C_2|, \tag{32}$$

where the individual components are given by

$$|C_0\rangle = \frac{1}{\sqrt{3}}(|\phi_{00}\rangle|\sqrt{\gamma}\alpha\rangle + |\phi_{02}\rangle|\sqrt{\gamma}\alpha e^{-2\pi i/3}\rangle + |\phi_{01}\rangle|\sqrt{\gamma}\alpha e^{2\pi i/3}\rangle), \tag{33}$$

$$|C_1\rangle = \frac{1}{\sqrt{3}}(|\phi_{20}\rangle|\sqrt{\gamma}\alpha\rangle + |\phi_{22}\rangle|\sqrt{\gamma}\alpha e^{-2\pi i/3}\rangle + |\phi_{21}\rangle|\sqrt{\gamma}\alpha e^{2\pi i/3}\rangle), \tag{34}$$

$$|C_2\rangle = \frac{1}{\sqrt{3}}(|\phi_{10}\rangle|\sqrt{\gamma}\alpha\rangle + |\phi_{12}\rangle|\sqrt{\gamma}\alpha e^{-2\pi i/3}\rangle + |\phi_{11}\rangle|\sqrt{\gamma}\alpha e^{2\pi i/3}\rangle), \tag{35}$$

with the two-qutrit Bell states from Eq. (22).

In order to obtain entanglement between the two matter systems, the coherent states $|\sqrt{\gamma}\alpha\rangle$, $|\sqrt{\gamma}\alpha e^{-2\pi i/3}\rangle$, and $|\sqrt{\gamma}\alpha e^{2\pi i/3}\rangle$ have to be distinguished (see Fig. 2). Like in the loss-free case, this can be done using a homodyne measurement on the light mode. Unlike the qubit case, an $\hat{x}$ measurement is not suitable here, because $|\sqrt{\gamma}\alpha e^{2\pi i/3}\rangle$ and $|\sqrt{\gamma}\alpha e^{-2\pi i/3}\rangle$ cannot be distinguished. Therefore, we choose the quadrature $\hat{p}$ whose Gaussian momentum distribution for coherent states with complex amplitude β reads

$$|\psi_\beta(p)|^2 = \sqrt{\frac{2}{\pi}}\exp\{-2[p - \text{Im}(\beta)]^2\}. \tag{36}$$

This time, it is useful to define at least three windows to which a measurement result is assigned when the light mode of the output state in Eq. (32) is measured (see Fig. 2). The first window is a symmetric interval around $p = 0$, $w_0 = [-\Delta, \Delta]$. A measurement result in this interval, similar to the qubit case, corresponds to an approximate projection on $|\sqrt{\gamma}\alpha\rangle$. A projection onto the states $|\sqrt{\gamma}\alpha e^{\pm 2\pi i/3}\rangle$ is assumed if a value falls into $w_1 = [\frac{\sqrt{3}}{2}\sqrt{\gamma}\alpha - \Delta, \infty]$ or $w_2 = [-\infty, -\frac{\sqrt{3}}{2}\sqrt{\gamma}\alpha + \Delta]$, respectively. Note that we need $\Delta \leqslant \frac{1}{2}\sqrt{\frac{3}{4}}\sqrt{\gamma}\alpha =: \Delta_0$ to exclude overlapping windows. We may decide to add two extra windows w_3 and w_4 to include the possibility of discarding measurement results (see Fig. 2). Inclusion of such failure events renders our qutrit entanglement distribution probabilistic.

Using the momentum wave functions for the coherent states, the qutrit-qutrit-qubus $|C_0\rangle$ component of ρ'_{out} after measuring the value p in the homodyne detection of the qubus has the conditional state for the two matter qutrits

$$\begin{aligned}\sigma_p^{C_0} = \text{Tr}_{qubus}(|p\rangle\langle p|C_0\rangle\langle C_0|p\rangle\langle p|) = \tfrac{1}{3}[&|\phi_{00}\rangle\langle\phi_{00}||\psi_{\sqrt{\gamma}\alpha}(p)|^2 + |\phi_{02}\rangle\langle\phi_{02}||\psi_{\sqrt{\gamma}\alpha e^{-2\pi i/3}}(p)|^2 + |\phi_{01}\rangle\langle\phi_{01}||\psi_{\sqrt{\gamma}\alpha e^{2\pi i/3}}(p)|^2 \\ &+ |\phi_{00}\rangle\langle\phi_{02}|\psi_{\sqrt{\gamma}\alpha}(p)\psi^*_{\sqrt{\gamma}\alpha e^{-2\pi i/3}}(p) + |\phi_{00}\rangle\langle\phi_{01}|\psi_{\sqrt{\gamma}\alpha}(p)\psi^*_{\sqrt{\gamma}\alpha e^{2\pi i/3}}(p) + |\phi_{02}\rangle\langle\phi_{00}|\psi_{\sqrt{\gamma}\alpha e^{-2\pi i/3}}(p)\psi^*_{\sqrt{\gamma}\alpha}(p) \\ &+ |\phi_{02}\rangle\langle\phi_{01}|\psi_{\sqrt{\gamma}\alpha e^{-2\pi i/3}}(p)\psi^*_{\sqrt{\gamma}\alpha e^{2\pi i/3}}(p) + |\phi_{01}\rangle\langle\phi_{00}|\psi_{\sqrt{\gamma}\alpha e^{2\pi i/3}}(p)\psi^*_{\sqrt{\gamma}\alpha}(p) + |\phi_{01}\rangle\langle\phi_{02}|\psi_{\sqrt{\gamma}\alpha e^{2\pi i/3}}(p)\psi^*_{\sqrt{\gamma}\alpha e^{-2\pi i/3}}(p)].\end{aligned} \tag{37}$$

If we only accept the selection window $w_0 = [-\Delta, \Delta]$, the resulting unnormalized state is obtained by doing the p integration

$$\sigma_{w_0}^{C_0} = \int_{-\Delta}^{\Delta} dp\, \sigma_p^{C_0}. \tag{38}$$

For carefully chosen α and L_0, the undesired off-diagonal parts of the density operator can be made very small and, similar to the qubit case [17], they will eventually quickly vanish after a few purification steps. Therefore we neglect these terms in the following, and obtain the unnormalized state

$$\tilde{\rho}_{w_0}^{C_0} = \frac{1}{3}\left(|\phi_{00}\rangle\langle\phi_{00}|\int_{-\Delta}^{\Delta} dp|\psi_{\sqrt{\gamma}\alpha}(p)|^2 + |\phi_{02}\rangle\langle\phi_{02}|\int_{-\Delta}^{\Delta} dp|\psi_{\sqrt{\gamma}\alpha e^{-2\pi i/3}}(p)|^2 + |\phi_{01}\rangle\langle\phi_{01}|\int_{-\Delta}^{\Delta} dp|\psi_{\sqrt{\gamma}\alpha e^{2\pi i/3}}(p)|^2\right). \tag{39}$$

The same calculation as above for $|C_0\rangle$ can be made for the other two components in ρ'_{out} of Eq. (32), $|C_1\rangle$ and $|C_2\rangle$. The total conditional (unnormalized) density matrix then becomes

$$\tilde{\rho}_{w_0} = \frac{N_u(\sqrt{1-\gamma}\alpha)}{9}\tilde{\rho}_{w_0}^{C_0} + \frac{N_v(\sqrt{1-\gamma}\alpha)}{9}\tilde{\rho}_{w_0}^{C_1} + \frac{N_w(\sqrt{1-\gamma}\alpha)}{9}\tilde{\rho}_{w_0}^{C_2}, \tag{40}$$

whose norm is the success probability

$$\begin{aligned} p_{w_0} &= \text{Tr}[\tilde{\rho}_{w_0}] \\ &= \frac{1}{3}\int_{-\Delta}^{\Delta} dp[|\psi_{\sqrt{\gamma}\alpha}(p)|^2 + |\psi_{\sqrt{\gamma}\alpha e^{-2\pi i/3}}(p)|^2 \\ &\quad + |\psi_{\sqrt{\gamma}\alpha e^{2\pi i/3}}(p)|^2], \end{aligned} \tag{41}$$

where we used $\text{Tr}[\rho'_{\text{out}}] = 1$ and $\text{Tr}[\tilde{\rho}_{w_0}^{C_0}] = \text{Tr}[\tilde{\rho}_{w_0}^{C_1}] = \text{Tr}[\tilde{\rho}_{w_0}^{C_2}]$. The corresponding fidelity for the target state is then calculated as

$$\begin{aligned} F_{w_0} &= \frac{\langle\phi_{00}|\tilde{\rho}_{w_0}|\phi_{00}\rangle}{p_{w_0}} \\ &= \frac{N_u(\sqrt{1-\gamma}\alpha)}{9}\,\frac{\frac{1}{3}\int_{-\Delta}^{\Delta} dp|\psi_{\sqrt{\gamma}\alpha}(p)|^2}{p_{w_0}}. \end{aligned} \tag{42}$$

The success probabilities for the other two selection windows are obtained in complete analogy,

$$\begin{aligned} p_{w_1} &= \frac{1}{3}\int_{(\sqrt{3}/2)\sqrt{\gamma}\alpha-\Delta}^{\infty} dp[|\psi_{\sqrt{\gamma}\alpha}(p)|^2 + |\psi_{\sqrt{\gamma}\alpha e^{-2\pi i/3}}(p)|^2 \\ &\quad + |\psi_{\sqrt{\gamma}\alpha e^{2\pi i/3}}(p)|^2], \\ p_{w_2} &= \frac{1}{3}\int_{-\infty}^{-(\sqrt{3}/2)\sqrt{\gamma}\alpha+\Delta} dp[|\psi_{\sqrt{\gamma}\alpha}(p)|^2 + |\psi_{\sqrt{\gamma}\alpha e^{-2\pi i/3}}(p)|^2 \\ &\quad + |\psi_{\sqrt{\gamma}\alpha e^{2\pi i/3}}(p)|^2]. \end{aligned} \tag{43}$$

The corresponding fidelities with respect to the target states $|\phi_{01}\rangle$ and $|\phi_{02}\rangle$ for these windows are, respectively,

$$F_{w_1} = \frac{N_u(\sqrt{1-\gamma}\alpha)}{9}\,\frac{\frac{1}{3}\int_{(\sqrt{3}/2)\sqrt{\gamma}\alpha-\Delta}^{\infty} |\psi_{\sqrt{\gamma}\alpha e^{2\pi i/3}}(p)|^2}{p_{w_1}} \tag{44}$$

and

$$F_{w_2} = \frac{N_u(\sqrt{1-\gamma}\alpha)}{9}\,\frac{\frac{1}{3}\int_{-\infty}^{-(\sqrt{3}/2)\sqrt{\gamma}\alpha+\Delta} |\psi_{\sqrt{\gamma}\alpha e^{-2\pi i/3}}(p)|^2}{p_{w_2}}. \tag{45}$$

To estimate the performance of this entanglement-generation scheme, we define the average fidelity as

$$F_{av} = \frac{\sum_{i=0}^{2} p_{w_i} F_{w_i}}{P_{\text{succ}}}, \tag{46}$$

where $P_{\text{succ}} = \sum_{i=0}^{2} p_{w_i}$ is the total success probability. The α dependence of the success probability and the average fidelity for various values of Δ is shown in Figs. 4 and 5 for $L_0 = 5$ km.

Clearly, if $\Delta = \Delta_0$, then there is no failure window at all and all measurement results are accepted. This corresponds to unit success probability $P_{\text{succ}} = 1$. On the other hand, for smaller (but not too small) Δ, i.e., $\Delta < \Delta_0$, the success probability still tends to unity for increasing α, as long as the three coherent states remain well within their respective selection windows. The fidelity, however, shows the opposite behavior. The smaller Δ is chosen, the higher the average fidelity for moderate values of α. Increasing α makes the fidelity finally drop to $1/3$, which is a direct consequence of the loss channel whose mixed output becomes more and more balanced for larger α. For each chosen value of Δ, there is an optimal value for α leading to a maximal fidelity. For instance, still with $L_0 = 5$ km, choosing $\Delta = 0.2\Delta_0$ and $\alpha \approx 1$ leads to an average fidelity of $F_{av} \approx 0.7$ at a very reasonable success probability of $P_{\text{succ}} \approx 0.4$. The corresponding plots for elementary distances of $L_0 = 10$ km are shown in Figs. 6 and 7.

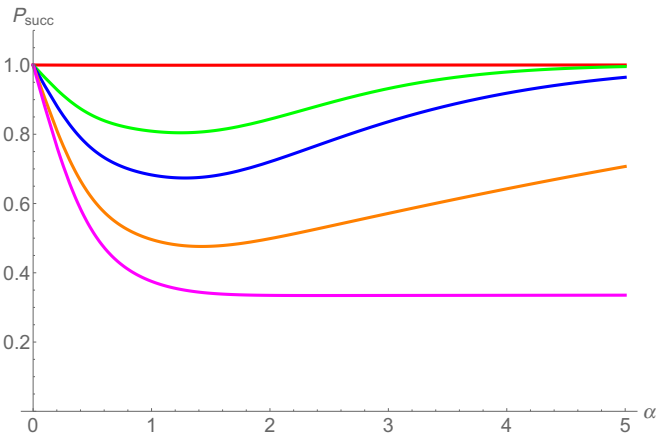

FIG. 4. Success probability for the homodyne-based distribution of qutrit-qutrit entanglement over a distance of 5 km for various Δ: $\Delta = \Delta_0$ (red line), $\Delta = 0.7\Delta_0$ (green line), $\Delta = 0.5\Delta_0$ (blue line), $\Delta = 0.2\Delta_0$ (orange line), and $\Delta = 0.001\Delta_0$ (magenta line) (from top to bottom).

E. Unambiguous state discrimination

In this section we consider an alternative measurement scheme for a qutrit hybrid repeater based upon so-called

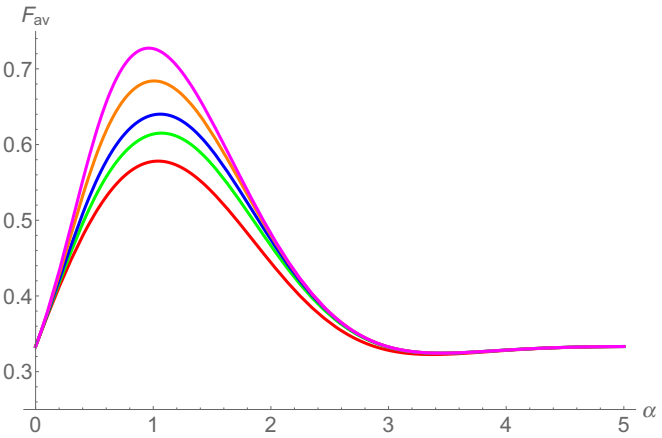

FIG. 5. Average fidelity for the homodyne-based distribution of qutrit-qutrit entanglement over a distance of 5 km for various Δ: $\Delta = \Delta_0$ (red line), $\Delta = 0.7\Delta_0$ (green line), $\Delta = 0.5\Delta_0$ (blue line), $\Delta = 0.2\Delta_0$ (orange line), and $\Delta = 0.001\Delta_0$ (magenta line) (from bottom to top).

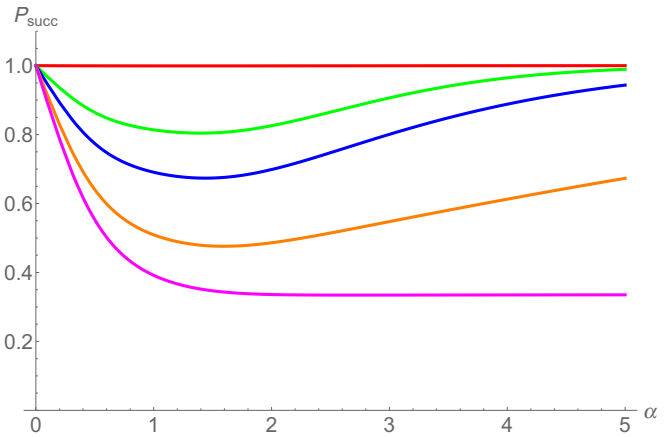

FIG. 6. Success probability for the homodyne-based distribution of qutrit-qutrit entanglement over a distance of 10 km for various Δ: $\Delta = \Delta_0$ (red line), $\Delta = 0.7\Delta_0$ (green line), $\Delta = 0.5\Delta_0$ (blue line), $\Delta = 0.2\Delta_0$ (orange line), and $\Delta = 0.001\Delta_0$ (magenta line) (from top to bottom).

unambiguous state discrimination. Compared to the homodyne-based scheme, the conceptual difference in the USD-based scheme is that the nonorthogonality of the coherent states only affects P_{succ} and no longer F_{av}, as USD enables one to discriminate nonorthogonal states probabilistically in an error-free fashion. The idea is that a successful and error-free projection onto one of the states $|\sqrt{\gamma}\alpha\rangle$ or $|\sqrt{\gamma}\alpha e^{\pm 2\pi i/3}\rangle$ would always lead to a maximally entangled state in the first component of Eq. (32). The task is therefore to find the most efficient possible scheme in the framework of quantum theory for unambiguously discriminating between the three coherent states above.

This problem was treated by Chefles [38], who derived the optimal success probability as

$$P_D \leqslant \min_r \sum_{j=0}^{2} e^{-2\pi i j r/3} e^{\gamma\alpha^2(e^{2\pi i j/3}-1)}, \tag{47}$$

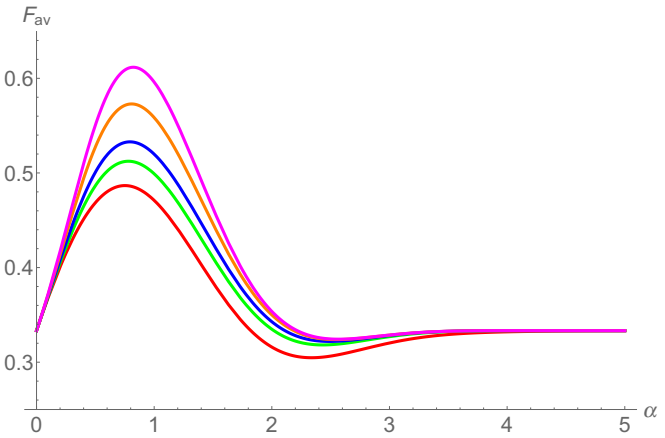

FIG. 7. Average fidelity for the homodyne-based distribution of qutrit-qutrit entanglement over a distance of 10 km for various Δ: $\Delta = \Delta_0$ (red line), $\Delta = 0.7\Delta_0$ (green line), $\Delta = 0.5\Delta_0$ (blue line), $\Delta = 0.2\Delta_0$ (orange line), and $\Delta = 0.001\Delta_0$ (magenta line) (from bottom to top).

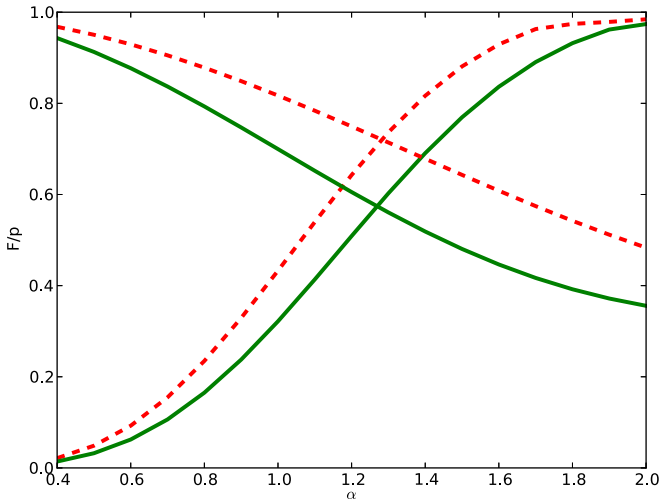

FIG. 8. Success probabilities (increasing with increasing α) and fidelities (decreasing with increasing α) for the USD-based scheme for 5 km (red dotted line) and 10 km (green solid line) dependent on α.

with $r = 0, 1, 2$ (see also Refs. [39,40]). The relation between this optimal probability and the corresponding fidelity of the final maximally entangled state is shown in Fig. 8.

F. Entanglement purification

Entanglement purification aims at generating fewer high-fidelity copies from many noisy copies of a certain pure target state via local operations and classical communication. By iterating this purification protocol, a fidelity arbitrarily close to unity can be achieved. The purification of mixed qubit states was investigated by Bennett *et al.* [41] for the class of Werner states [42]. Nearly at the same time, Deutsch *et al.* [43] demonstrated a similar purification protocol for states diagonal in the Bell basis. Both protocols require only two copies for each step with Deutsch's scheme, leading to a better efficiency compared to the Bennett scheme. The latter was demonstrated experimentally [44,45] and also generalized to arbitrary dimensions [46,47].

As shown in the next two sections for both USD and homodyne detection, we deal in both cases with Bell-diagonal mixed quantum states beyond qubits. Therefore, we choose a qudit generalization of the Deutsch protocol presented in [48] for the purification step. Because of the different arising output states to be purified, we treat USD and homodyne detection separately.

1. USD

Since USD perfectly distinguishes between the three coherent states $|\sqrt{\gamma}\alpha\rangle$ and $|\sqrt{\gamma}\alpha e^{\pm 2\pi i/3}\rangle$, the exact final state on the repeater segment for a projection onto, for instance, $|\sqrt{\gamma}\alpha\rangle$ reads as

$$\rho_{\text{eff}} = \frac{N_u(\sqrt{1-\gamma}\alpha)}{9}|\phi_{00}\rangle\langle\phi_{00}| + \frac{N_v(\sqrt{1-\gamma}\alpha)}{9}|\phi_{10}\rangle\langle\phi_{10}| + \frac{N_w(\sqrt{1-\gamma}\alpha)}{9}|\phi_{20}\rangle\langle\phi_{20}|, \tag{48}$$

where, as defined earlier,

$$\begin{aligned}|\phi_{00}\rangle &= \frac{1}{\sqrt{3}}(|00\rangle + |11\rangle + |22\rangle),\\ |\phi_{10}\rangle &= \frac{1}{\sqrt{3}}(|00\rangle + e^{-2\pi i/3}|11\rangle + e^{2\pi i/3}|22\rangle),\\ |\phi_{20}\rangle &= \frac{1}{\sqrt{3}}(|00\rangle + e^{2\pi i/3}|11\rangle + e^{-2\pi i/3}|22\rangle).\end{aligned} \tag{49}$$

To perform a purification of this state, i.e., to increase the statistical weight of $|\phi_{00}\rangle$ in Eq. (48), at least two copies of the matter-matter output state are required. The protocol in [48] in this case works as follows: The first matter-qutrit system is subject to the transformation

$$\begin{aligned}|0\rangle &\mapsto \frac{1}{\sqrt{3}}(|0\rangle + |1\rangle + |2\rangle),\\ |1\rangle &\mapsto \frac{1}{\sqrt{3}}(|0\rangle + e^{i\phi}|1\rangle + e^{-i\phi}|2\rangle),\\ |2\rangle &\mapsto \frac{1}{\sqrt{3}}(|0\rangle + e^{-i\phi}|1\rangle + e^{i\phi}|2\rangle),\end{aligned} \tag{50}$$

while on the second system

$$\begin{aligned}|0\rangle &\mapsto \frac{1}{\sqrt{3}}(|0\rangle + |1\rangle + |2\rangle),\\ |1\rangle &\mapsto \frac{1}{\sqrt{3}}(|0\rangle + e^{-i\phi}|1\rangle + e^{i\phi}|2\rangle),\\ |2\rangle &\mapsto \frac{1}{\sqrt{3}}(|0\rangle + e^{i\phi}|1\rangle + e^{-i\phi}|2\rangle)\end{aligned} \tag{51}$$

is performed where $\phi = \frac{2\pi}{3}$. The components of the mixture are then transformed as

$$\begin{aligned}|\phi_{00}\rangle \mapsto |\phi_{00}\rangle &= \frac{1}{\sqrt{3}}(|00\rangle + |11\rangle + |22\rangle),\\ |\phi_{10}\rangle \mapsto |\phi_{01}\rangle &= \frac{1}{\sqrt{3}}(|01\rangle + |12\rangle + |20\rangle),\\ |\phi_{20}\rangle \mapsto |\phi_{02}\rangle &= \frac{1}{\sqrt{3}}(|10\rangle + |21\rangle + |02\rangle).\end{aligned} \tag{52}$$

A mixture of $|\phi_{00}\rangle$, $|\phi_{01}\rangle$, and $|\phi_{02}\rangle$ with statistical weights p_0, p_1, and p_2, where $p_0 + p_1 + p_2 = 1$, can now be purified using the purification scheme of [48]. Note that the purification of the state in Eq. (48) can be considered as a qutrit version of [44,45]: One takes two copies of the state that is shared between two parties A and B. Local subtraction gates are applied on the qutrits belonging to A and B before A and B select one of the two copies and measure its respective spin. Equal spin results lead to the new mixed state

$$\rho' = \frac{\sum_{j=0}^{2} p_j^2 |\phi_{0j}\rangle\langle\phi_{0j}|}{\sum_{j=0}^{2} p_j^2}, \tag{53}$$

whose fidelity with respect to the target state $|\tilde{D}_0\rangle$ is now increased, provided $p_0 > 1/3$ and $p_1, p_2 < p_0$.

2. Homodyne scheme

After the homodyne detection, the conditional state resulting from Eq. (32) also represents a mixed state. Depending on the channel distance, the selection window, and the amplitude α, the resulting state in the first component is a mixture of the dominant target state $|\phi_{00}\rangle$ with small extra components of $|\phi_{02}\rangle$ and $|\phi_{01}\rangle$ (if the result belongs to window w_0). Furthermore, small off-diagonal terms appear which will be neglected. This is similar for the other two components of the mixture with their rotated Bell states. The resulting total state is therefore treated as Bell diagonal of the form

$$\rho = \sum_{k,j=0}^{2} A_{kj} |\phi_{kj}\rangle\langle\phi_{kj}| \tag{54}$$

with some statistical weights A_{kj} for all nine Bell states dependent on the measurement result. Compared to USD, error terms appear and have to be taken into account. The purification scheme presented in [48] can nevertheless deal with this situation. The scheme works again with two copies of the state in Eq. (54). Local subtraction gates are applied and finally spin measurements are performed. Equal spin results give the state

$$\rho' = \frac{\sum_{j,k,g} A_{kj} A_{gj} |\phi_{k\oplus g,j}\rangle\langle\phi_{k\oplus g,j}|}{\sum_{j,k,g} A_{kj} A_{gj}} \tag{55}$$

with success probability

$$p_3 = \sum_{j,k,g} A_{kj} A_{gj}$$

and increased fidelity depending on the initial statistical weights. Note that $\oplus$ denotes addition modulo 3.

G. Entanglement swapping

In the previous sections we have shown how to entangle two qutrits over a distance L_0. The distance L_0, however, is typically too short for general applications in quantum communication. It is therefore necessary to further extend the entanglement over larger distances. This can be done by entanglement swapping.

To perform entanglement swapping, two entangled qutrit-qutrit pairs are generated next to each other, covering a total distance of $2L_0$. To connect the two pairs and thus distribute entanglement over twice the initial distance, a Bell measurement is carried out on the two adjacent matter systems. A successful Bell measurement projects the remaining two matter systems onto a maximally entangled state.

In analogy to the qubit case, a Bell measurement on two qutrits can be performed by applying a qudit sum gate (CNOT or CSHIFT), followed by measurements in the X and in the Z basis [see Eq. (18)]. As pointed out in [49], Hadamard transformations and a CPHASE gate suffice to implement the sum gate. In the following, we assume that arbitrary single-qutrit rotations and measurements can be performed on the matter systems and show how to construct the sum gate based on these assumptions.

In our framework, a CPHASE gate is represented by the unitary operation

$$U_{CP} = \exp\left(-\frac{2\pi i}{3} S_{z_1}^{(3)} S_{z_2}^{(3)}\right), \tag{56}$$

where the operators $S_{z_i}^{(3)}$ correspond to the operations introduced in Eq. (18) on the ith qutrit. Like in the qubit case of a CNOT gate, a decomposition for the qudit CSHIFT gate is given by

$$\text{CSHIFT} = (H \otimes \mathbb{1})\,\text{CPHASE}(H \otimes \mathbb{1}), \tag{57}$$

where H is the qutrit Hadamard transformation. Indeed, one observes by direct calculation $(H \otimes \mathbb{1})\,\text{CPHASE}(H \otimes \mathbb{1})|x, y\rangle = |x \ominus y, y\rangle$ for $x, y \in \mathbb{Z}_2$. Note that $\ominus$ denotes subtraction modulo 3. A more formal proof of this decomposition for arbitrary dimensions is given in Sec. IV. With HQR protocols for qubits and qutrits in mind, an extension to higher dimensions, e.g., four-level systems (ququarts), is straightforward.

H. Rate analysis

1. Methods and assumptions

In this section we quantify the performance of our qutrit HQR protocol for the generation of entanglement over the total channel distance L. The performance can be assessed by the entanglement-generation rate, i.e., the number of entangled pairs over the entire distance per unit time. Besides this, the fidelity of the generated states is of particular interest.

The atomic matter systems also serve as quantum memories (as needed because of the probabilistic step of entanglement purification after the entanglement distribution) and we assume matter systems with infinite coherence time, i.e., perfect memories. In addition, we assume deterministic and error-free gates on them. In particular, the entanglement swapping operation is treated as deterministic, employing the gates as described in the preceding section. Strictly speaking, photon transmission loss is the only error source entering our rate analysis and the resulting rates have to be understood as upper bounds of the actual achievable rates. For this scenario, analytical formulas for the rates dependent on the number of elementary segments as well as the number of purifications performed on each segment after the distributions have been derived in [50]. Note that we include one to several rounds of entanglement purification only right after the initial entangled-state distributions. In this theoretical treatment, our repeater scheme effectively becomes a second generation quantum repeater (recall Sec. I) where rates are ultimately limited by $R \lesssim \frac{c}{L_0}$ (instead of $R \lesssim \frac{c}{L}$ if purifications were performed until the final nesting level [1,2]) [4,5].

We consider 2^n segments of elementary distance L_0, covering a total distance $L = 2^n L_0$. Entanglement is generated in each segment with a probability P_0. If the obtained state is not directly purified, the resulting rate becomes

$$R_n = \frac{c}{2L_0}\frac{1}{Z_n(P_0)} = \frac{1}{T_0 Z_n(P_0)}, \tag{58}$$

where

$$Z_n(P_0) = \sum_{j=1}^{2^n} \binom{2^n}{j} \frac{(-1)^{j+1}}{1-(1-P_0)^j} \tag{59}$$

is the average total number of attempts it takes for all segments to eventually share an entangled pair (recall that initially shared pairs can be stored as long as needed), $T_0 = \frac{2L_0}{c}$ is the elementary time unit for sending the quantum states and also the classical information to confirm their successful distribution (as well as purification), and c is the speed of light in the optical fiber.

If one round of purification is performed, the same formula can be applied, but now P_0 has to be substituted by an effective probability

$$Q_1(L_0) = P_0 P_1\left(\frac{2-P_0}{3-2P_0}\right), \tag{60}$$

where P_1 is the probability for the first round of purification to succeed. Furthermore, the rates with two and three rounds of purification can be calculated using the effective probabilities

$$Q_2(L_0) = Q_1(L_0) P_2\left(\frac{2-Q_1(L_0)}{3-2Q_1(L_0)}\right) \tag{61}$$

and

$$Q_3(L_0) = Q_2(L_0) P_3\left(\frac{2-Q_2(L_0)}{3-2Q_2(L_0)}\right), \tag{62}$$

where P_2 and P_3 are the success probabilities for two and three rounds of purification, respectively. Note that without the use of quantum memories, Q_3 would scale as $P_0^8 P_1^4 P_2^2 P_3$, which (assuming small probabilities) is turned into a scaling like $P_0 P_1 P_2 P_3$ with the help of the quantum memories. Higher rounds of purification can be considered in a recursive fashion. We analyze the rates for the USD- and homodyne-based scheme separately in the next two sections.

2. USD-based scheme

For the USD scheme, P_0 is given by the optimal probability in Eq. (47) to distinguish the three coherent states $|\sqrt{\gamma}\alpha\rangle$ and $|\sqrt{\gamma}\alpha e^{\pm 2\pi i/3}\rangle$. For $|\sqrt{\gamma}\alpha\rangle$, the resulting state is given by Eq. (48) and the initial fidelity of the target state reads

$$F_0 = \frac{N_u(\sqrt{1-\gamma}\alpha)}{9} \tag{63}$$

with

$$F_1 = \frac{N_v(\sqrt{1-\gamma}\alpha)}{9}, \quad F_2 = \frac{N_w(\sqrt{1-\gamma}\alpha)}{9} \tag{64}$$

for the other two components (and hence the infidelity $F_1 + F_2$ with regard to the desired state). One round of purification succeeds with probability

$$P_1 = F_0^2 + F_1^2 + F_2^2 \tag{65}$$

and the resulting improved fidelity is

$$F_0' = \frac{F_0^2}{F_0^2 + F_1^2 + F_2^2}. \tag{66}$$

For more rounds of purification, the fidelities and success probabilities can be obtained recursively. After entanglement swapping, the final fidelity of the entangled state distributed over the total distance is lower bounded by $(\tilde{F}_0)^{2^n}$, where $\tilde{F}_0$ is the final fidelity for each segment, possibly obtained after some rounds of purification.

3. Homodyne-based scheme

An exact rate analysis for the HQR with entanglement distribution based on homodyne detection is much more demanding than for the USD case. This is due to the fact that at adjacent elementary segment potentially different mixed quantum states are generated depending on the corresponding measurement result. As already pointed out, these states can be brought into a similar form, i.e., the components are equal, but the statistical weights are not necessarily equal. An exact rate analysis is therefore out of reach.

To nevertheless assess the performance of that scheme, we model the situation with an effective state on each elementary segment. This effective state has the average fidelity $F_{av}(\alpha,\gamma)$ as the statistical weight of the first component (target Bell state $|\phi_{00}\rangle$), whereas the other two components are equally weighted with $F_i = \frac{1}{8}[1 - F_{av}(\alpha,\gamma)]$ for $i = 2, 3, \ldots, 8$. This effectively corresponds to a model of white noise on the matter systems which is often an acceptable approximation.

For an elementary distance of $L_0 = 5$ km, we choose $\alpha \approx 1$, which leads to a maximum initial fidelity of approximately 0.7. As the generation probability P_0 we insert the success probability $P_{\text{succ}} = \sum_{i=0}^{2} p_{w_i}$ for obtaining a result in one of the success windows (see Sec. III D) which equals approximately 0.4 in this case. For $L_0 = 10$ km, we also have $\alpha \approx 1$, but now $F_{av} \approx 0.6$, which requires many rounds of purification and does not lead to reasonable rates anymore.

Using these initial values, the formulas for the rates and fidelities, including some possible rounds of purification, can directly be applied. For quantitative examples and an illustration of the trade-off between repeater rates and fidelities, see the Appendix.

To summarize some of the results presented there, for elementary distances as short as $L_0 = 5$ km, the USD-based scheme performs better than the homodyne-based scheme for both success probability and total fidelity. In the case of USD, at least three rounds of purification are needed in order to obtain reasonable fidelities and rates for distances as large as 640 km. For the homodyne scheme, such total distances already require five and more rounds of purification.

Results for a situation with a more practical repeater spacing, $L_0 = 20$ km, indicate that for $L = 1280$ km near-unit fidelities at rates on the order of hertz are only achievable using USD, because in the homodyne-based scheme the initial output fidelities are very low and therefore an impractical number of rounds of purification are required (this also leads to extremely low rates). Note that a similar observation was made for the original qubit scheme based on homodyne detection [17].

IV. GENERAL QUDIT CASE

Based on the results obtained in the preceding sections for specific examples, we now in turn propose HQR protocols for arbitrary finite-dimensional quantum systems.

The dispersive interaction between a general qudit, i.e., a d-level system, and a light mode can be realized by the Hamiltonian

$$H_{\text{int}}^{(d)} = \hbar g S_z^{(d)} a^\dagger a, \tag{67}$$

with $S_z^{(d)}|k\rangle = (\frac{2k-d+1}{2})|k\rangle$ for $k = \{0, 1, \ldots, d-1\}$ and where $S_z^{(2)} = \sigma_z$. The corresponding unitary is $U_d(\theta) = \exp(i\theta S_z^{(d)} a^\dagger a)$ and the relevant case of a strong interaction is obtained by setting $\theta = \frac{2\pi}{d}$.

The first step in the protocol is the preparation of the matter state $\frac{1}{\sqrt{d}}\sum_{k=0}^{d-1}|k\rangle$, which then interacts with an optical coherent state $|\alpha\rangle$ via the strong dispersive interaction. This results in a hybrid entangled qudit-light (qudit-qubus) state

$$\frac{1}{\sqrt{d}}\sum_{k=0}^{d-1}|k\rangle|\alpha e^{2\pi ik/d}\rangle. \tag{68}$$

After locally generating qudit-light entanglement, the light mode is sent through an optical channel of length L_0 where it is subject to photon loss. Including again an ancilla vacuum mode and mixing it with the optical mode results in

$$\frac{1}{\sqrt{d}}\sum_{q=0}^{d-1}|q\rangle|\sqrt{\gamma}\alpha e^{2\pi iq/d}\rangle|\sqrt{1-\gamma}\alpha e^{2\pi iq/d}\rangle. \tag{69}$$

As in the specific examples above, the crucial point is now to find a suitable basis for tracing out the loss mode. Here, in the general case, this basis consists of the d vectors

$$|v_m\rangle = \frac{1}{\sqrt{N_{v_m}(\alpha)}}\sum_{k=0}^{d-1} e^{2\pi ikm/d}|\alpha e^{2\pi ik/d}\rangle, \tag{70}$$

with $m = 0, 1, \ldots, d-1$. We can thus recast the coherent states of the ancilla light mode in Eq. (69) as

$$|\alpha e^{2\pi ik/d}\rangle = \frac{1}{d}\sum_{m=0}^{d-1}\sqrt{N_{v_m}(\alpha)}e^{-2\pi ikm/d}|v_m\rangle \tag{71}$$

and find, for Eq. (69),

$$\frac{1}{d\sqrt{d}}\sum_{q,m=0}^{d-1}\sqrt{N_{v_m}(\sqrt{1-\gamma}\alpha)}e^{-2\pi iqm/d}|q\rangle|\sqrt{\gamma}\alpha e^{2\pi iq/d}\rangle|v_m\rangle. \tag{72}$$

Tracing out the loss mode in this basis is now a trivial task and one obtains

$$\rho_{\text{out}} = \sum_{m=0}^{d-1}\frac{N_{v_m}(\sqrt{1-\gamma}\alpha)}{d^2} \times\left[\left(\frac{1}{\sqrt{d}}\sum_{q=0}^{d-1}e^{-2\pi iqm/d}|q\rangle|\sqrt{\gamma}\alpha e^{2\pi iq/d}\rangle\right)\times\text{H.c.}\right] \tag{73}$$

for the d-component qudit-light output state.

Again, this can be further simplified by basis transformations on both the light mode and the matter system. The light mode can be expressed in the basis given in Eq. (70), while the matter system can be written in the (generalized Pauli) qudit X basis

$$|\tilde{k}\rangle = \frac{1}{\sqrt{d}}\sum_{m=0}^{d-1}e^{2\pi ikm/d}|m\rangle \tag{74}$$

for $k = 0, 1, \ldots, d-1$. This gives the expression

$$\rho_{\text{out}} = \sum_{m=0}^{d-1} \frac{N_{v_m}(\sqrt{1-\gamma}\alpha)}{d^2} \times \left[\left(\frac{1}{d} \sum_{r=0}^{d-1} \sqrt{N_{v_r}} |m \tilde{\oplus} r\rangle |\tilde{v}_r\rangle \right) \text{H.c.} \right] \tag{75}$$

for Eq. (73), where $\oplus$ denotes addition modulo d. Note that a tilde again indicates basis vectors with damped amplitude $\sqrt{\gamma}\alpha$ on the light mode and the X basis on the matter system.

After traveling through the loss channel over a distance L_0, the light mode reaches a second matter system, also prepared in the state $\frac{1}{\sqrt{d}} \sum_{k=0}^{d-1} |k\rangle$. The light mode interacts dispersively with the second matter system, this time with the inverse angle $\theta = -\frac{2\pi}{d}$. The resulting state becomes

$$\rho = \sum_{m=0}^{d-1} \frac{N_{v_m}}{d^2} |T_m\rangle\langle T_m|, \tag{76}$$

with the components

$$|T_m\rangle = \frac{1}{d} \sum_{q=0}^{d-1} \sum_{l=0}^{d-1} e^{-2\pi i q m/d} |q\rangle |l\rangle |\sqrt{\gamma}\alpha e^{2\pi i (q-l)/d}\rangle, \tag{77}$$

written in the original basis [like in Eq. (73)].

The state discrimination in the general case involves the d coherent states $|\sqrt{\gamma}\alpha\rangle, \ldots, |\sqrt{\gamma}\alpha e^{2\pi i(d-1)/d}\rangle$, which can be graphically represented as coherent states "on a ring" (see Fig. 9 for $d = 8$). A projection onto one of the d coherent states collapses each component onto a maximally entangled state. However, by increasing the dimension d, a projection scheme based on homodyne detection becomes more and more futile since no direction is uniquely specified anymore. A scheme for unambiguously discriminating exactly these d coherent states was derived in [38] for arbitrary dimensions (for $d = 3$, recall Sec. III E). An upper bound for the success probability is given by

$$P_D \leqslant \min_r \sum_{j=0}^{d-1} e^{-2\pi i j r/d} e^{\gamma\alpha^2 (e^{2\pi i j/d} - 1)}, \tag{78}$$

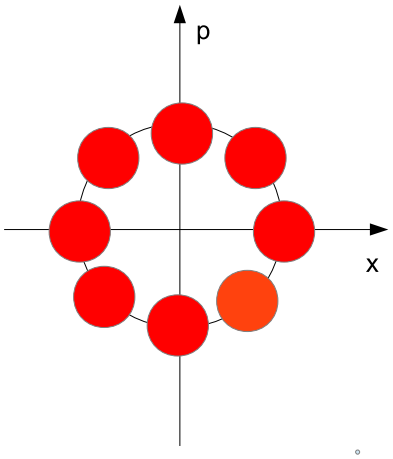

FIG. 9. Phase-space representation of the qubus mode for $d = 8$.

$r = 0, 1, \ldots, d-1$, where Eq. (47) is recovered for $d = 3$. Since the upper bound on the right-hand side depends on both α and γ, the minimization with respect to r is hard analytically. We therefore calculate the bound numerically.

After the USD, the resulting mixed state will be a mixture of d maximally entangled Bell states of the form ($k = 0, \ldots, d-1$)

$$|\phi_{kj}\rangle = \frac{1}{\sqrt{d}} \sum_{y=0}^{d-1} e^{2\pi i k y/d} |y, y \ominus j\rangle \tag{79}$$

for one fixed $j = 0, \ldots, d-1$, according to the specific identified coherent state (here $\ominus$ denotes subtraction modulo d). For example, in the qutrit case $d = 3$, the result $j = 0$ corresponds to identifying $|\sqrt{\gamma}\alpha\rangle$ and the three Bell states in the mixture are given by Eq. (49). If $j \neq 0$, a j-fold application of $X = \sum_{k=0}^{d-1} |k+1\rangle\langle k|$ transforms all these states to

$$|\phi_{k0}\rangle = \frac{1}{\sqrt{d}} \sum_{y=0}^{d-1} e^{2\pi i k y/d} |y, y\rangle. \tag{80}$$

By means of local unitaries, the different components of the mixtures with $|\phi_{k0}\rangle$ can always be transformed to a mixture of the states

$$|\psi_j\rangle \equiv |\phi_{0j}\rangle = \frac{1}{\sqrt{d}} \sum_{y=0}^{d-1} |y, y \ominus j\rangle, \tag{81}$$

with now all j included. We therefore obtain

$$\rho = \sum_{j=0}^{d-1} p_j |\psi_j\rangle\langle\psi_j| \tag{82}$$

for the state to be purified.

The purification now works as follows. We prepare two copies of the state in Eq. (82) such that the total joint four-qudit state reads

$$\rho \otimes \rho = \sum_{j=0}^{d-1} \sum_{k=0}^{d-1} p_j p_k |\psi_j\rangle|\psi_k\rangle\langle\psi_j|\langle\psi_k|, \tag{83}$$

where the individual terms are

$$|\psi_j\rangle|\psi_k\rangle = \frac{1}{d} \sum_{y=0}^{d-1} \sum_{y'=0}^{d-1} |y, y \ominus j\rangle |y', y' \ominus k\rangle. \tag{84}$$

One applies a local CSHIFT gate on systems 1 and 3 as well 2 and 4 in order to obtain

$$\frac{1}{d} \sum_{y=0}^{d-1} \sum_{y'=0}^{d-1} |y - y', y \ominus y' \oplus k \ominus j\rangle |y', y' \ominus k\rangle. \tag{85}$$

After that, the first spins of the first two systems are measured. If the spins are parallel, it follows $k = j$ such that only diagonal parts contribute. As a consequence, the second two

systems collapse to $|\psi_k\rangle$. The new state then becomes

$$\rho' = \frac{\sum_{j=0}^{d-1} p_j^2 |\psi_j\rangle\langle\psi_j|}{\sum_{j=0}^{d-1} p_j^2}. \tag{86}$$

The fidelity with respect to the target state $|\psi_0\rangle$ is thus

$$F' = \frac{p_0^2}{\sum_{j=0}^{d-1} p_j^2}, \tag{87}$$

which is increased compared to the initial fidelity p_0 if $p_0 > \frac{1}{d}$ and $p_i < p_0$ for $i = 1, \ldots, d-1$.

After possibly several rounds of purification, a high-fidelity entangled state can be obtained between the two separated qudits. This is referred to as the initial entanglement generation or distribution.

To further extend the entanglement, two elementary segments next to each other are connected via entanglement swapping through Bell measurements on adjacent repeater nodes, i.e., a projection on maximally entangled qudit-qudit states. Generalizing the qutrit case, we show that the CSHIFT gate lies at the heart of such Bell measurements and that these can be realized by a CPHASE gate based on the generalized dispersive interaction.

The CPHASE gate for an arbitrary dimension d is realized by the two-qudit unitary transformation

$$U_d = \exp\left(-\frac{2\pi i}{d} S_{z_1}^{(d)} S_{z_2}^{(d)}\right), \tag{88}$$

with the generalized spin operator $S_i^{(d)}$ acting on qudit i. We show by direct calculation that the sequence $H \otimes 1 \rightarrow$ CPHASE $\rightarrow H \otimes 1$ acts as a controlled phase shift gate on an arbitrary two-qudit state:

$$\begin{aligned}
&(H \otimes 1)\text{CPHASE}(H \otimes 1)|xy\rangle \\
&= (H \otimes 1)\text{CPHASE}\frac{1}{\sqrt{d}}\sum_{k=0}^{d-1}\exp\left(\frac{2\pi i k x}{d}\right)|ky\rangle \\
&= (H \otimes 1)\frac{1}{\sqrt{d}}\sum_{k=0}^{d-1}\exp\left(\frac{2\pi i k (x-y)}{d}\right)|ky\rangle \\
&= |x-y, y\rangle.
\end{aligned} \tag{89}$$

Together with arbitrary qudit rotations and measurements in the qudit X and Z basis, this suffices to implement a deterministic Bell state analyzer for qudits [49].

V. DISCUSSION AND CONCLUSIONS

We introduced a hybrid quantum repeater protocol for the distribution of arbitrary finite-dimensional bipartite entangled states over large distances with a specific focus on qutrit entanglement. A generalization of the dispersive light-matter interaction from the qubit to the general qudit case lies at the heart of our protocol and can be expressed by higher spin operators. The distribution of matter-matter entanglement between neighboring repeater stations is mediated via coherent states interacting dispersively and subsequently with the matter systems. We investigated both USD and homodyne detection of the light mode and compared the rates and final fidelities. By exploiting purification on the elementary segments, sufficiently high initial fidelities can be achieved to cover distances up to 640 km (homodyne) and 1280 km (USD) with final fidelities close to unity. With three rounds of entanglement purification directly after the initial entanglement distributions, rates ∼100 Hz are, in principle, possible in the case of USD.

The idealizations made in this paper with respect to perfect matter memories and gate operations are undoubtedly experimentally demanding to approach (i.e., to emulate by sufficiently good memories and gates), but clearly lead to upper bounds on both the success probabilities and fidelities. On the other hand, no repeater schemes currently exist for the distribution of qudit-qudit entanglement. In particular,

TABLE I. Results on the rates and fidelities for $L_0 = 5$ km (USD), $\alpha = 1.2$, and $L \leqslant 640$ km.

	Rounds of purification	none	one	two	three
	Initial fidelity	0.75	0.944	0.998	∼1
Distance (km)	Effective probability	0.64	0.30	0.19	0.13
	Rate (Hz)				
10		10175	4290	2647	900
20		7936	3185	1942	656
40		6366	2488	1506	507
80		5285	2024	1220	409
160		4501	1701	1021	342
320		3914	1464	877	294
640		3461	1284	768	257
	Fidelity				
10		0.56	0.891	0.996	0.999993
20		0.315	0.793	0.991	0.999985
40		0.09	0.63	0.983	0.99997
80		0	0.397	0.966	0.99994
160		0	0.158	0.934	0.9998
320		0	0.02	0.872	0.9997
640		0	0	0.761	0.9995

TABLE II. Results on the rates and fidelities for $L_0 = 10$ km (USD), $\alpha = 1.2$, and $L \leqslant 1280$ km.

	Rounds of purification	none	one	two	three
	Initial fidelity	0.652	0.87	0.987	0.999
Distance (km)	Effective probability	0.414	0.147	0.078	0.05
	Rate (Hz)				
20		3020	1010	524	343
40		2271	738	380	248
80		1788	570	293	191
160		1463	461	236	156
320		1234	385	197	128
640		1065	331	169	110
1280		936	289	147	96
	Fidelity				
20		0.420	0.76	0.974	0.999
40		0.18	0.57	0.95	0.999
80		0.03	0.33	0.9	0,999
160		0.001	0.1	0.814	0.998
320		0	0.01	0.66	0.996
640		0	0	0.436	0.992
1280		0	0	0.19	0.984

TABLE III. Results on the rates and fidelities for $L_0 = 5$ km (homodyne), $\alpha \approx 1$, and $L \leqslant 640$ km.

	Rounds of purification	none	one	two	three	four	five
	Initial fidelity	0.730	0.815	0.954	0.964	0.998	0.999
Distance (km)	Effective probability	0.38	0.180	0.087	0.055	0.035	0.023
			Rate (Hz)				
10		5496	2487	1173	744	466	311
20		4117	1823	852	539	336	225
40		3233	1412	656	414	258	172
80		2641	1143	529	334	208	139
160		2225	957	442	279	173	116
320		1919	821	379	239	148	99
640		1686	719	331	208	130	86
			Fidelity				
10		0.53	0.66	0.91	0.93	0.997	0.997
20		0.28	0.44	0.83	0.87	0.995	0.995
40		0.08	0.195	0.684	0.75	0.989	0.990
80		0.01	0.04	0.47	0.56	0.979	0.979
160		0	0	0.22	0.32	0.959	0.959
320		0	0	0.05	0.1	0.920	0.921
640		0	0	0	0.01	0.84	0.85

standard click-based protocols such as the DLCZ scheme [9] do not exist for qudits and it has even been shown that such schemes are unrealizable for the most common and convenient types of encoding (see [51]). Therefore, we believe that our scheme can serve as an in-principle version of a genuine beyond-qubit quantum repeater, in which case it seems justified to first consider channel loss as the absolutely dominating error contribution [provided one can expect a sufficiently little (though nonzero) error contribution from the local gates and operations that does not entirely spoil the repeater's scaling].

Since our scheme assumes perfect matter systems (with perfect coherence properties for sufficiently long times) and operations on them, future research may aim at investigating different physical platforms and the specific decoherence models for these matter systems. Like for the qubit case [52], quantum error correction codes could be employed on the matter systems turning the scheme to a genuine second-generation quantum repeater scheme and thus preserving the communication rates obtained here under idealizing assumptions.

ACKNOWLEDGMENTS

We acknowledge support from Q.com (BMBF).

APPENDIX: RATE ANALYSIS FOR THE QUTRIT HYBRID QUANTUM REPEATER

In this Appendix, we show Tables I–IV summarizing the results on the rates and fidelities for our qutrit quantum

TABLE IV. Results on the rates and fidelities for $L_0 = 20$ km (USD), $\alpha = 0.5$, and $L \leqslant 1280$ km.

	Rounds of purification	none	one	two
	Initial fidelity	0.862	0.986	0.9998
Distance (km)	Effective probability	0.014	0.007	0.004
		Rate (Hz)		
40		92	46	30
80		33	17	11
160		26	13	9
320		21	11	7
640		17	9	6
1280		15	8	5
		Fidelity		
20		0.862	0.986	0.9999
40		0.743	0.973	0.9998
80		0.552	0.946	0.9995
160		0.304	0.895	0.999
320		0.093	0.802	0.998
640		0.009	0.643	0.996
1280		0	0.413	0.992

repeater scheme ($d = 3$), as described in Sec. III H. We consider various total distances up to 1280 km, two possible elementary distances ($L_0 = 5, 10$ km), between zero and three rounds of entanglement purification directly after the initial entanglement distribution, and the two possible detection schemes (homodyne and USD).

[1] H.-J. Briegel, W. Dür, J. I. Cirac, and P. Zoller, Phys. Rev. Lett. **81**, 5932 (1998).

[2] W. Dür, H.-J. Briegel, J. I. Cirac, and P. Zoller, Phys. Rev. A **59**, 169 (1999).

[3] N. Sangouard, C. Simon, H. de Riedmatten, and N. Gisin, Rev. Mod. Phys. **83**, 33 (2011).

[4] S. Muralidharan, L. Li, J. Kim, N. Lütkenhaus, M. D. Lukin, and L. Jiang, Sci. Rep. **6**, 20463 (2016).

[5] S. Muralidharan, J. Kim, N. Lütkenhaus, M. D. Lukin, and L. Jiang, Phys. Rev. Lett. **112**, 250501 (2014).

[6] F. Ewert, M. Bergmann, and P. van Loock, Phys. Rev. Lett. **117**, 210501 (2016).

[7] F. Ewert and P. van Loock, Phys. Rev. A **95**, 012327 (2017).

[8] M. Żukowski, A. Zeilinger, M. A. Horne, and A. K. Ekert, Phys. Rev. Lett. **71**, 4287 (1993).

[9] L.-M. Duan, M. D. Lukin, J. I. Cirac, and P. Zoller, Nature (London) **414**, 413 (2001).

[10] W. J. Munro, A. M. Stephens, S. J. Devitt, K. A. Harrison, and K. Nemoto, Nat. Photon. **6**, 777 (2012).

[11] K. Azuma, K. Tamaki, and H.-K. Lo, Nat. Commun. **6**, 6787 (2015).

[12] M. Takeoka, S. Guha, and M. M. Wilde, Nat. Commun. **5**, 5235 (2014).

[13] S. Pirandola, R. Laurenza, C. Ottaviani, and L. Banchi, Nat. Commun. **8**, 15043 (2017).

[14] A brief chronological summary of the different contributions to the secret-key agreement capacity can be found in footnote [32] of Ref. [53]. Note that the bounds of point-to-point quantum communication can be exceeded without quantum memories or quantum error correction with one middle station at which two laser fields interfere [54] or incoming photons are multiplexed and conditionally connected depending on their nondestructive detections [55]. These schemes give a square root improvement of the effective transmission parameter and have not been shown to be more scalable.

[15] Y.-W. Cho, G. T. Campbell, J. L. Everett, J. Bernu, D. B. Higginbottom, M. T. Cao, J. Geng, N. P. Robins, P. K. Lam, and B. C. Buchler, Optica **3**, 100 (2016).

[16] P. van Loock, N. Lütkenhaus, W. J. Munro, and K. Nemoto, Phys. Rev. A **78**, 062319 (2008).

[17] P. van Loock, T. D. Ladd, K. Sanaka, F. Yamaguchi, K. Nemoto, W. J. Munro, and Y. Yamamoto, Phys. Rev. Lett. **96**, 240501 (2006).

[18] T. D. Ladd, P. van Loock, K. Nemoto, W. J. Munro, and Y. Yamamoto, New J. Phys. **8**, 184 (2006).

[19] U. L. Andersen, J. S. Neergaard-Nielsen, P. van Loock, and A. Furusawa, Nat. Phys. **11**, 713 (2015).

[20] A. D. Pfister, M. Salz, M. Hettrich, U. G. Poschinger, and F. Schmidt-Kaler, Appl. Phys. B **122**, 89 (2016).

[21] J. B. Brask, I. Rigas, E. S. Polzik, U. L. Andersen, and A. S. Sørensen, Phys. Rev. Lett. **105**, 160501 (2010).

[22] Y. Lim, J. Joo, T. P. Spiller, and H. Jeong, Phys. Rev. A **94**, 062337 (2016).

[23] T. Vértesi, S. Pironio, and N. Brunner, Phys. Rev. Lett. **104**, 060401 (2010).

[24] H.-P. Lo, C.-M. Li, A. Yabushita, Y.-N. Chen, C.-W. Luo, and T. Kobayashi, Sci. Rep. **6**, 22088 (2016).

[25] N. J. Cerf, M. Bourennane, A. Karlsson, and N. Gisin, Phys. Rev. Lett. **88**, 127902 (2002).

[26] V. Scarani, H. Bechmann-Pasquinucci, N. J. Cerf, M. Dušek, N. Lütkenhaus, and M. Peev, Rev. Mod. Phys. **81**, 1301 (2009).

[27] M. Erhard, R. Fickler, M. Krenn, and A. Zeilinger, Light: Sci. Appl. **7**, 17146 (2018).

[28] E. T. Jaynes and F. W. Cummings, Proc. IEEE **51**, 89 (1963).

[29] C. Gerry and P. Knight, *Introductory Quantum Optics* (Cambridge University Press, Cambridge, 2005).

[30] M. B. Plenio and S. Virmani, Quantum Inf. Comput. **7**, 1 (2007).

[31] O. Gühne and G. Tóth, Phys. Rep. **474**, 1 (2009).

[32] R. Horodecki, P. Horodecki, M. Horodecki, and K. Horodecki, Rev. Mod. Phys. **81**, 865 (2009).

[33] K. Banaszek, Phys. Lett. A **253**, 12 (1999).

[34] Z. Gedik, I. A. Silva, B. Çakmak, G. Karpat, E. L. G. Vidoto, D. O. Soares-Pinto, E. R. deAzevedo, and F. F. Fanchini, Scientific Reports **5**, 14671 (2015).

[35] S. Dogra, K. Dorai, and Arvind, Phys. Lett. A **380**, 1941 (2016).

[36] G. Vidal and R. F. Werner, Phys. Rev. A **65**, 032314 (2002).

[37] M. B. Plenio, Phys. Rev. Lett. **95**, 090503 (2005).

[38] A. Chefles, Phys. Lett. A **239**, 339 (1998).

[39] S. J. van Enk, Phys. Rev. A **66**, 042313 (2002).

[40] S. Croke, S. M. Barnett, and G. Weir, Phys. Rev. A **95**, 052308 (2017).

[41] C. H. Bennett, G. Brassard, S. Popescu, B. Schumacher, J. A. Smolin, and W. K. Wootters, Phys. Rev. Lett. **78**, 2031 (1997).

[42] R. F. Werner, Phys. Rev. A **40**, 4277 (1989).

[43] D. Deutsch, A. Ekert, R. Jozsa, C. Macchiavello, S. Popescu, and A. Sanpera, Phys. Rev. Lett. **77**, 2818 (1996).

[44] J.-W. Pan, C. Simon, C. Brukner, and A. Zeilinger, Nature (London) **410**, 1067 (2001).

[45] J.-W. Pan, S. Gasparoni, R. Ursin, G. Weihs, and A. Zeilinger, Nature (London) **423**, 417 (2003).

[46] M. Horodecki and P. Horodecki, Phys. Rev. A **59**, 4206 (1999).

[47] G. Alber, A. Delgado, N. Gisin, and I. Jex, J. Phys. A: Math. Gen. **34**, 8821 (2001).

[48] M. A. Martín-Delgado and M. Navascués, Eur. Phys. J. D **27**, 169 (2003).

[49] M. Dušek, Opt. Commun. **199**, 161 (2001).

[50] N. K. Bernardes, L. Praxmeyer, and P. van Loock, Phys. Rev. A **83**, 012323 (2011).

[51] J. Calsamiglia, Phys. Rev. A **65**, 030301 (2002).

[52] N. K. Bernardes and P. van Loock, Phys. Rev. A **86**, 052301 (2012).

[53] M. Pant, H. Krovi, D. Towsley, L. Tassiulas, L. Jiang, P. Basu, D. Englund, and S. Guha, arXiv:1708.07142.

[54] M. Lucamarini, Z. L. Yuan, J. F. Dynes, and A. J. Shields, Nature (London) **557**, 400 (2018).

[55] K. Azuma, K. Tamaki, and W. J. Munro, Nat. Commun. **6**, 10171 (2015).